RSC Advances

ROYAL SOCIETY OF CHEMISTRY

www.rsc.org/advances

Electrochemical and *in situ* ATR – SEIRAS Investigations of Methanol and CO Electro-oxidation on PVP-free Cubic and Octahedral/Tetrahedral Pt Nanoparticles

Augusta M. Levendorf, De-Jun Chen, Christopher L. Rom, Yangwei Liu, and YuYe J. Tong *

Department of Chemistry, Georgetown University, 37th & O Street NW,
Washington DC, 20057 (USA)
Tel: 202-687-5872; Fax: 202-687-5591
*E-mail: yyt@georgetown.edu

Abstract

Most wet-chemical methods that synthesize metal nanoparticles (NPs) of a particular size and desired shape include the use of a stabilizing surfactant, such as poly(vinylpyrrolidone) (PVP). The latter has the ability to prohibit and/or promote surface sites from participating in electrocatalytic reactions, *i.e.* the methanol oxidation reaction (MOR). In light of our recent findings that adsorbed PVP can enhance the MOR on Pt NPs, a strong effort was made herein to separate the NP surface orientation effect from that of surface-bound PVP. We report the *in situ* ATR-SEIRAS (attenuated total reflection-surface enhanced infrared reflection absorption spectroscopy) and electrochemical (EC) studies of MOR and CO oxidation reaction (COR) performed on PVP-free cubic and octahedral/tetrahedral (O/T) Pt NPs that were obtained using an adapted liquid phase UV photo-oxidation (UVPO) technique. Transmission electron microscope (TEM) images showed no observable changes of shape and size after the elimination of the PVP, while the integrity of the atomic surface structure was further confirmed by the orientation-dependent EC stripping analysis of irreversibly adsorbed adatoms, *i.e.* Bi and Ge. The MOR activity was enhanced by the preferential surface orientation of the O/T Pt NPs compared to commercial Pt black and the cubic Pt NPs. The *in situ* ATR-SEIRAS measurements showed that the PVP-free Pt NPs adsorbed more bridge-bound gaseous CO than those with residual PVP and the weakly hydrogen-bound interfacial water played an important role for the orientation dependent enhancement in MOR activity. Additionally, the findings of this work are coupled with previously published investigations regarding the influence that PVP exerts on the ultimate activity of the Pt NPs, i.e., the adsorbed PVP enhances further the MOR activity on the O/T but suppresses it on the cubic Pt NPs.

1. Introduction

Among the various small alcohol fuel cells, which efficiently convert chemical energy into electrical energy, the direct methanol fuel cell (DMFC) offers promising technical advantages in terms of energy density and facile fuel distribution for future implementation.[1-3] Single crystal Pt studies have served as the foundation for understanding the methanol oxidation reaction (MOR) occurring at the anode, which is sensitive to the surface morphology as defined by the exposed crystallographic planes.[2, 4, 5] These single crystal studies have established that the activity for MOR in acidic media, *i.e*. $HClO_4$ or H_2SO_4, increases in the order of Pt(111) < Pt (110) < Pt(100) for the bulk surfaces. In practice, however, metallic nanoparticles (NPs) are the economically viable form of electrocatalysts for catalyzing DMFC reactions in fuel cells because they offer an efficient way of utilizing expensive materials due to large surface area to volume ratios and unique catalytic properties due to their reduced dimensions.[6] Extrapolating the results obtained on macroscopic single crystal surfaces to the nanoscale electrocatalysts, however, is not as straightforward as it appears since the reduced dimensions of metal NPs can introduce unexpected geometric and electronic effects that can alter substantially the catalytic behavior of the exposed nanofacets.[7-9] For example, the MOR trends in acidic media on Pt NPs are different from the trends observed on bulk crystals, *i.e.* the activity increases in the order of Pt NPs enclosed by Pt(100) < Pt(110) < Pt(111) nanofacets.[8, 10]

Since the pioneering work of El-Sayed *et al.* in 1996 to synthesize preferentially shape-controlled Pt NPs, sophisticated investigations by Feliu *et al*., Sun *et al*. and others continue to elucidate the relationships between structure and catalytic activity at the nanoscale as well as correlations between macroscopic and nanoscopic systems.[9-15] The advances in NP research allow NPs of unique shapes and sizes to be synthesized from a diverse array of techniques ranging from thermal decomposition to potentiometric methods.[9, 14, 16] In the polyol-based

synthetic approaches, surfactants are frequently used as size stabilizing and/or shape-controlling agents, where poly(vinylpyrrolidone) (PVP) is among the most popular used. Following the synthesis, the remaining surface-site-blocking surfactants are usually considered reaction inhibitors and consequently become the targets of elimination. The eradication of PVP without damaging the structural integrity of the NPs has been a challenging endeavor for the community.[17-19]

In addition to synthetic control of the shape that has been correlated qualitatively to the exposed crystallographic planes via TEM, evaluating the atomic arrangement at the surface quantitatively is of paramount importance.[6] Among the detailed electrochemical (EC) investigations reported by Feliu *et al.*, they have developed methods that allow for *in situ* characterization of the surface order using irreversible adatom adsorption that more accurately describes the surface atomic arrangement.[10, 12, 20]

In view of the recent investigations that adsorbed PVP can improve the MOR on Pt through surface water activation and an enhanced direct pathway,[21, 22] more specifically, an unexpected large enhancement in MOR was observed on the octahedral/tetrahedral (O/T) Pt NPs that had ~16wt% residual PVP after a strong base treatment.[8] Our subsequent studies[21, 22] have also shown that adsorbing PVP onto Pt black and carbon-supported Pt NPs can substantially enhance the MOR and formic acid oxidation reaction activities. In this follow-up study to recently published works focused on PVP-protected NPs, we investigate whether the MOR activity enhancement observed on these PVP-protected systems is purely a PVP induced effect or a combination of the former with the surface orientation effect at nanoscale.[8, 33]This paper reports the results obtained from the EC and *in situ* SEIRAS (surface enhanced IR reflection absorption spectroscopy) investigations of MOR and carbon monoxide (CO) oxidation reaction (COR) performed on the PVP-free cubic and O/T Pt NPs.. The shape-controlled Pt NPs were

synthesized employing an established polyol method that uses PVP as the size stabilizer as done previously, however we were able to achieve complete removal of surface-bound PVP with an optimized liquid phase UV treatment combined with oxygenated H_2O_2 (UVPO).[17, 19] TEM and adatom adsorption that will be discussed later, were used to qualitatively and quantitatively probe the atomic surface arrangement of the Pt NPs to ensure structural integrity prior to the EC and *in situ* SEIRAS measurements.

2. Materials and Methods

2.1. Synthesis of Shape-Controlled Pt NPs. The shape-controlled Pt NPs of ~11 nm were synthesized in a one-step procedure according to the established polyol based procedures as done previously.[23, 24] In a round bottom flask, 2.5 mL of ethylene glycol (EG) was refluxed for *ca*. 20 min. Subsequently, 0.5 mL of 0.002 M or 0.06 M $AgNO_3$ in EG were added to the boiling EG in order to achieve Pt (100) bound NPs (cubes) or Pt (111) bound NPs (octahedrons/tetrahedrons), respectively. Alternating 94 μL of 0.375 M PVP (55,000 M_w – 3 mL total) and 47μL of 0.0675M $H_2PtCl_6 \cdot 6H_2O$ (1.5 mL total) in EG were added to the boiling EG solution at 30s intervals. The reaction solution was refluxed for an additional 10 min then allowed to cool to room temperature.

In general, the reaction solution was centrifuged for 20 min at 6000 rpm to remove the AgCl precipitate if required. In order to remove the excess EG and PVP, the supernatant was centrifuged with a triple volume of acetone for 20 min at 6000 rpm until the NCs were clearly separated. The resulting Pt NPs was dispersed into *ca.* 5 mL EtOH via sonication and then 20 mL of hexanes were added before centrifugation for 20 min at 6000 rpm, which was repeated at least 3 times until final dispersion into EtOH.

A modified procedure of liquid phase UV combined with oxygenated H_2O_2 (UVPO) was optimized to remove the residual PVP from the surface.[17, 19] Briefly, a small proportion of the ethanolic-suspension of NPs was dispersed into about 2 mL of H_2O with 200 - 250 mg NaOH to yield a basic environment. Separately, a basic solution of 10 mL of H_2O_2 was prepared by adding 200 - 250 mg NaOH and then the solution was bubbled for at least 10 min with O_2 gas. The basic solution of NPs underwent UV irradiation (254 nm) for 1 hr with the addition of *ca.* 1 mL of O_2-saturated H_2O_2 solution at specific time intervals, *i.e.* every 10 min. After UV exposure, the resultant solution was purified by the repetitive centrifugation and precipitation process with EtOH and ultimately dispersed in EtOH before drying overnight in the oven at 60°C.

2.2. Transmission Electron Microscopy (TEM). The resultant NPs were characterized by a JEOL-2100 LaB_6 microscope at the Nanoscale Imaging and Spectroscopy Laboratory at UMD College Park. Shape and size distributions were based on a minimum of 150 counts with the aid of the ImageJ software.

2.3. Thermogravimetric Analysis (TGA). TGA experiments were performed on a SDTQ600 or Q50 TA Instrument. The data was analyzed with Universal TA Analysis 2000 software to determine weight percent of PVP on the particle surface. Typically, at least 2 mg of sample was placed into a ceramic pan at room temperature (RT) before the temperature was increased at a rate of 10˚C min^{-1} to a minimum of 600˚C under a steady flow of nitrogen (20 mL min^{-1}).

2.4. Electrochemical (EC) Analysis. EC measurements were performed in an Ar-blanketed conventional three electrode EC cell using a CHI potentiostat (CH Instrument, Inc) that was controlled with CHI software. The supporting electrolyte solution was 0.5 M H_2SO_4 (GFS Chemicals, Double Distilled). Commercial Ag/AgCl (1 M) (CH Instrument, Inc) and Pt gauze electrodes were used as the reference and counter electrodes, respectively. The working electrode was comprised of NPs that were deposited onto a well-polished 3-mm commercial glassy carbon

electrode (GCE) (BioAnalytical Systems, Inc). The NP deposition involved a dilute suspension of NPs in water, usually 2 mg mL^{-1} that was drop cast onto the GCE and allowed to air dry.

Cyclic voltammetry (CV) and chronoamperometry (CA) were commonly used to assess the electrocatalytic activity of the samples. CVs were recorded with a 50 mV s^{-1} scan rate unless otherwise stated. The electrode potentials are given in reference to the reversible hydrogen electrode (RHE), although all data were collected using the Ag/AgCl reference electrode. The currents reported are normalized with respect to the Pt electrochemical surface area (ECSA) determined by the hydrogen desorption charge per area. The charge densities, based on Pt single crystal measurements, were 220, 208 and 240 μC cm^{-2} for polycrystalline, (100) and (111) atomic arrangements, respectively.[25]

The atomic surface structure was also investigated using the aforementioned irreversible adsorption of Bi or Ge, the details of which can be found elsewhere.[10, 20] In brief, Bi was spontaneously adsorbed onto a freshly rinsed Pt sample by immersion into a 0.001 M Bi_2O_3 in 0.6 M $HClO_4$ then placed into the EC cell at 0.3 V after being rinsed. Similarly, the rinsed sample was immersed into a 0.01 M GeO_2 in 1.0 M NaOH solution to adsorb Ge, but the electrode was not rinsed following adsorption. In each case, the sample was first cycled in 0.5 M H_2SO_4 below 0.9 V to achieve a stable CV, then cycled up to 1.0 V for 2 cycles and finally cycled with an upper potential of 0.9 V before adsorption of Bi or Ge. The adsorption experiments were performed in triplicate on the Pt black, cubic NPs and O/T NPs for each adatom.

In a typical catalytic experiment, the blank CV was recorded in a potential window until a stable curve was obtained in the supporting electrolyte. For the shape controlled NPs, it was important to minimize the surface restructuring due to oxide formation, thus the potential limit was 0.9 V_{RHE} prior to further measurements. Oxidation of adsorbed gaseous CO was performed

by holding the potential at 0.3 V while first saturating the electrolyte with CO gas for 5-10 min, then purging the solution with Ar gas for 15-25 min. Finally, a CV was recorded within a specific potential window to oxidize or strip the CO from the Pt surface. CV was employed to measure the intrinsic activity of the Pt NPs for the MOR at 0.5 M CH_3OH concentrations in the supporting electrolytes described above. Following the MOR CV, the CA current was measured over a 30 min period with the potential held at 0.5 V in the CH_3OH-containing electrolyte solution. Lastly, a CV was collected in pure electrolyte to ensure catalyst stability.

2.5. Attenuated Total Reflection (ATR)-Surface Enhanced Infrared Refection Adsorption Spectroscopy (ATR-SEIRAS). The ATR-SEIRAS measurements were collected on a Bruker Vector-22 IR Spectrometer that was modified to house an EC apparatus.[26-28] The *in situ* EC measurements were performed in a modified three electrode EC cell using a potentiostat (CH Instrument, Inc) that was controlled by a computer with CHI software. Commercial Ag/AgCl (1 M) (CH Instrument, Inc) and Pt gauze electrodes were used as the reference and counter electrodes, respectively. The working electrode was comprised of a well-polished Si prism that had a thin Au film chemically deposited onto one surface.[29] The NP catalysts were deposited directly onto the Au film as onto the GCE described above. The potential difference spectra were collected during a potential stair step experiment over the designated potential range. The spectra are shown in the absorbance units defined as $-\log (I - I_R)/I_R$, where I and I_R are the spectra taken at the measured and the reference potentials, respectively. The electrocatalysts were monitored between the potential-step experiments via CV in order to ensure that the system was stable.

3. Results and discussion

3.1. Physical Characterization. Size and shape distributions of the synthesized Pt NPs are displayed in Figure 1 along with representative TEM images. The shape of the NPs suggests the

existence of preferential surface planes, *i.e.* the cubic NPs display (100) planes, whereas O/T NPs exhibit (111) planes. The average size of the cubic and O/T Pt NPs were 10.9 ± 1.4 nm and 11.6 ± 2.0 nm, respectively, with over 70% yield of the desired shape obtained. More specifically, 71.2% of the NPs from the cubic sample were cubes with (100) facets, while 73.2% of the O/T sample were either octahedrons or tetrahedrons with (111) facets.

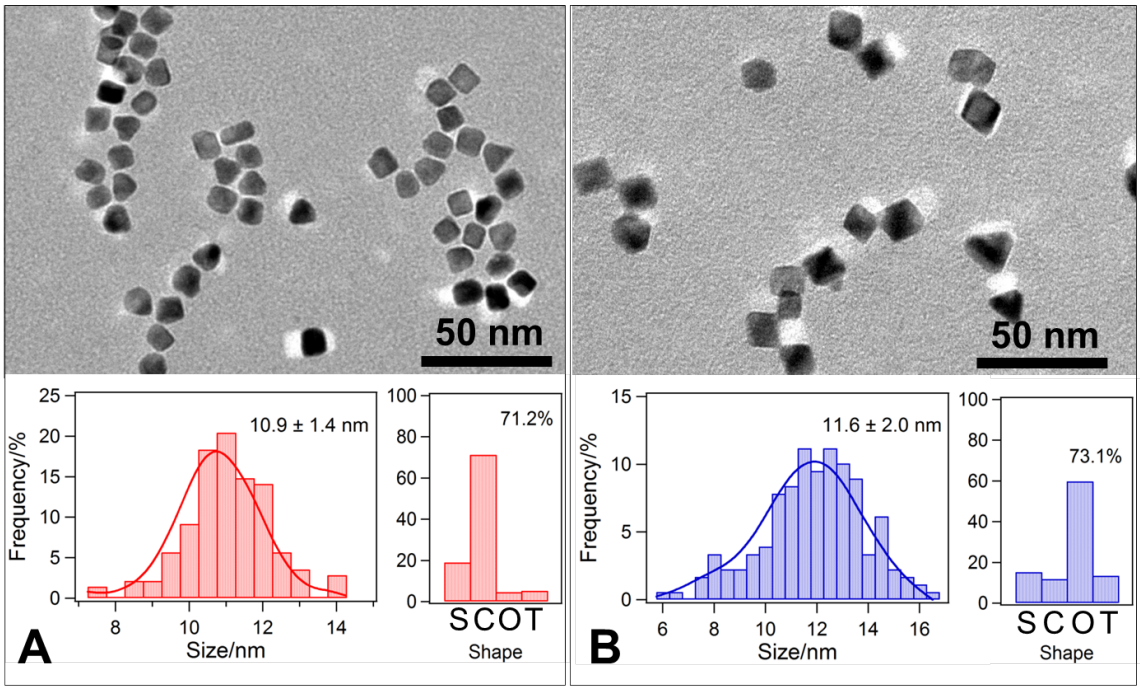

Figure 1. Representative TEM images of the cubic Pt NPs (A) and O/T NPs (B) synthesized along with size and shape distributions based on a minimum of 150 counts. S, C, O and T denote spherical and random shapes, cubes, octahedrons and tetrahedrons, respectively.

The high degree of monodispersity of the synthesized NPs in Figure 1 is attributed to the presence of PVP during the synthesis. Using thermal analysis, the weight loss due to the decomposition and/or desorption of the PVP as a function of increasing temperature provides insight into the amount of PVP present on the NP, *i.e.* surface-bound and vicinal units of the polymer . Figure 2 summarizes the TGA measurements performed on the as-synthesized and UVPO treated Pt NPs. Pure PVP desorbs between 400 and 450°C in the TGA as indicated by the inset of Figure 2B. Thus, the surfactant accounts for 7wt% and 12wt% on the as-synthesized

cubic and O/T Pt NPs as seen by the weight loss from 375 to 425°C in Figure 2A. Following the adapted liquid phase UVPO treatment, the NPs in Figure 2B exhibit no major weight loss in this temperature range expected for the desorption of PVP, which strongly suggests that no polymer was present on the surfaces and were similar to as-received commercial Pt black.

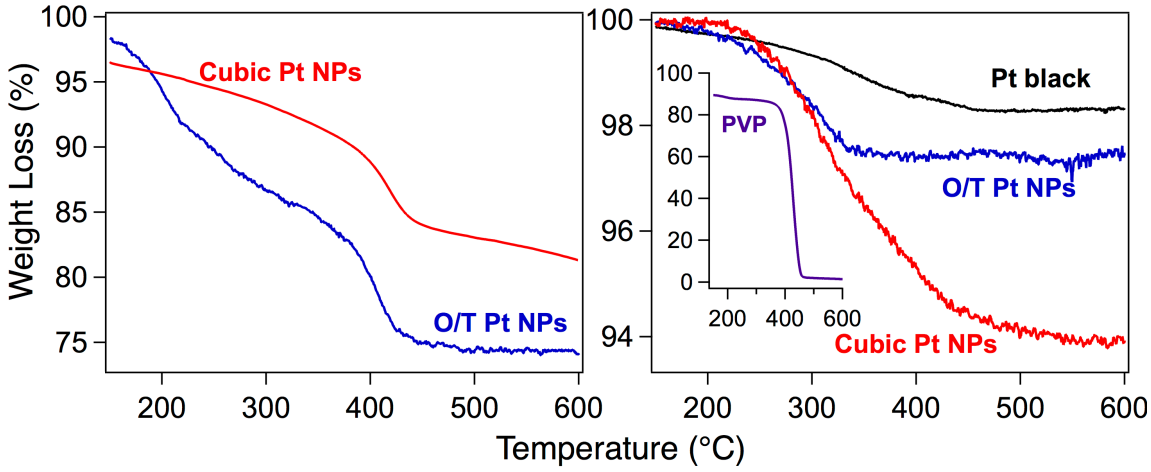

Figure 2. TGA curves of as-synthesized (A) and UVPO treated (B) cubic (red) and O/T (blue) Pt NPs along with the unaltered Pt black (black). The inset of B displays the TGA curve for pure PVP (purple), which highlights the absence of PVP weight loss at 400 to 450°C on the UVPO treated compared to the 7 wt% and 12 wt% presence of PVP on the as-synthesized cubic and O/T Pt NPs, respectively (A).

Despite the effectiveness of the UVPO method at removing the surface-bound PVP, the adverse effect of UV exposure on the surface atomic arrangement has been cautioned in the literature.[18, 30] There were no observable changes of the size and shape of the NPs before and after the UVPO treatment as noted by the TEM measurements, although the particles became more agglomerated. As mentioned shape suggests surface arrangement of the NPs only qualitatively and is by no means a quantitative description for the surface atomic arrangement.[30] Moreover, TEM is an *ex situ* method with a sample size that is much smaller than the number of NPs that are used for electrocatalysis. In order to measure the Pt surface structure more quantitatively, we adopted the irreversible adsorption/EC stripping methods developed by Feliu *et al*.[10, 12, 20]

CV was performed on the Pt black, cubic and O/T Pt NPs in 0.5 M H_2SO_4 to quantitatively infer the surface structure based on the charge distribution of peaks related to hydrogen and the (bi)sulfate adsorptions on various sites. The CV profiles for the samples in Figure 3A are normalized using single crystal hydrogen charge density values of 220, 208 and 240 μC cm^{-2} for polycrystalline, (100) and (111) atomic arrangements of Pt, respectively.[25] Foremost, the symmetry and clearly defined peaks on each sample in Figure 3A further supports the cleanliness of the samples, especially the synthesized NPs because surfactants tend to eliminate the sharpness of the associated peaks as previously reported.[22, 24, 31]

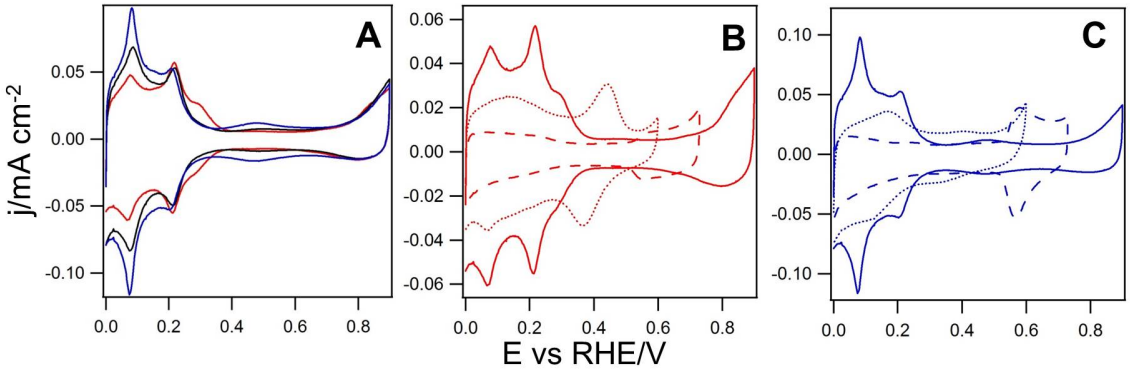

Figure 3. A. CVs of the Pt black (black), cubic (red) and O/T Pt NPs (blue) (A) in 0.5 M H_2SO_4. Comparison of CV profiles of pristine (solid) cubic (B) and O/T (C) Pt NPs with CVs after germanium (dot) and bismuth (dash) adsorption in 0.5 M H_2SO_4.

Upon visual inspection of Figure 3A, there are four principal peaks, whose charges depend on the exposed surface structure.[20, 24] The dominant peaks at *ca.* 0.09 V and *ca.* 0.22 V on Pt black are associated with hydrogen redox processes on (110)- and (100)-like step sites, whereas the hump around 0.5 V is indicative of (bi)sulfate adsorption on ordered (111) terrace domains. The increase of the hump at *ca.* 0.5 V on the O/T Pt NPs corresponds nicely to the presumed increase of (111) facets due to their shape. Moreover, the relative increase at the (110)-like step sites, which occur at step sites nearby (111) terrace domains, and negligible change at the (100) sites due to edges and corners demonstrates the preferential orientation of the surface as (111)

facets. In contrast, the cubic Pt NPs show hardly any anion adsorption current hump at ~0.5V indicating the absence of the (111) terrace domains, which is further confirmed by the decrease of the current peak related to the (110)-like step sites and increase of the current assigned to the (100)-like sites. Furthermore, the presence of the current shoulder at *ca.* 0.3 V indicates the increase in (100) terrace sites that are absent on the Pt black and O/T Pt NPs. Qualitatively, the charge distribution of the CV results approximates that indeed the atomic surface structure corresponds with the shape of the NPs.

For a more quantitative analysis of the atomic arrangements, the NPs were probed *in situ* using the irreversible adatom adsorption of Bi and Ge.[20] As described in the literature, the charge of the Bi redox peak occurring at *ca.* 0.58 V is proportional to the number of (111) terrace sites, and likewise, the charge from Ge at *ca.* 0.46 V is related to the (100) terrace sites. The CV results for the cubic and O/T Pt NPs are displayed in Figure 3B and 3C, respectively. The propensity for Bi to adsorb more on the O/T Pt NPs and less on the cubic NPs, while the inverse was observed for Ge adsorption, is the additional confirmation to the preferential surface structure obtained. Following the necessary adjustments, the charge of adatom adsorption/stripping is correlated to the hydrogen charge of the original CV results, which provides a percentage of the adatoms on different surface sites, *i.e.* the surface structure.

Figure 4 presents the HRTEM images of individual shaped NPs and the quantitative results of adatom adsorption measurements, clearly indicating that the shape controlled NPs were dominantly composed of the desired facets. More specifically, the cubic Pt NPs are *ca.* 40% comprised of the (100) terrace sites, which are nearly double the number of the (111) sites. Meanwhile, the O/T Pt NPs show *ca.* 50% being the (111) terrace sites. For comparison, the adatoms were adsorbed on the Pt black, which exhibited no preference for the terrace sites to the same degree as the synthesized NPs. Moreover, a qualitative inspection of the hydrogen charge

distributions in Figures 3 for the Pt NPs yields a similar conclusion for preferred surface arrangements. Therefore, these UV treated NPs were used as the preferentially oriented, PVP-free electrocatalysts for this work due to the absence of PVP and strong evidence for the desired atomic arrangements.

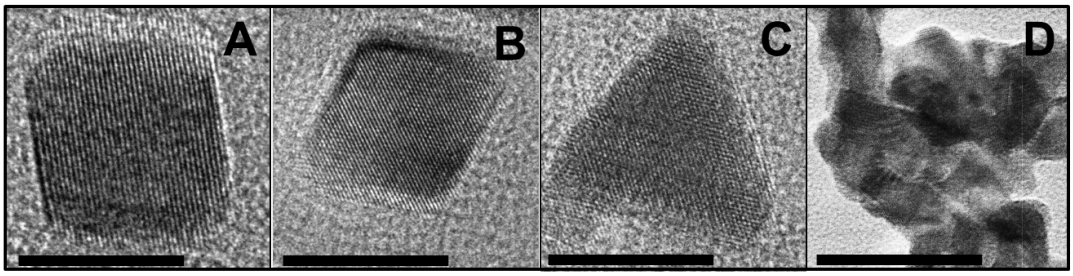

	[a]Size (nm)	[a]Shape (%)	[b]$(111)_t$ sites (%)	[c]$(100)_t$ sites (%)
Pt{111} NCs	11.6 ± 2.0	73.1	49.9 ± 7.3	4.6 ± 2.5
Pt{100} NCs	10.9 ± 1.4	71.2	22.4 ± 1.5	39.7 ± 1.1
Pt black	N/A	N/A	7.2 ± 5.1	12.0 ± 2.5

[a]Based on minimum of 150 counts
[b]Based on Bi adsorption on Pt(111)
[c]Based on Ge adsorption on Pt(100)
**Scale bar 10 nm*

Figure 4. A cubic (A), octahedral (B), and tetrahedral (C) Pt NP compared to the Pt black (D) with 10 nm scale bars. The tabulated results for Mean size and desired shape percentage of the NPs based on TEM images along with percentage of the (111) and (100) terrace sites on the NP ensembles based on irreversible adsorption of Bi onto the (111) and Ge onto the (100) sites, respectively.

3.2. Catalytic Activity Characterization. The normal CVs for the Pt black, cubic and O/T Pt NPs in 0.5 M H_2SO_4 are displayed in Figure 5A, respectively, which are reproduced from Figure 3A for facilitating the discussion. As described above, the dominant (110)-like and (100)-like step sites occur at *ca.* 0.09 V and *ca.* 0.22 V on Pt in 0.5M H_2SO_4, while the hump at *ca.* 0.5 V is indicative of anion adsorption on the (111) terrace domains and the bump at *ca.* 0.3 V is characteristic of (100) terrace domain.

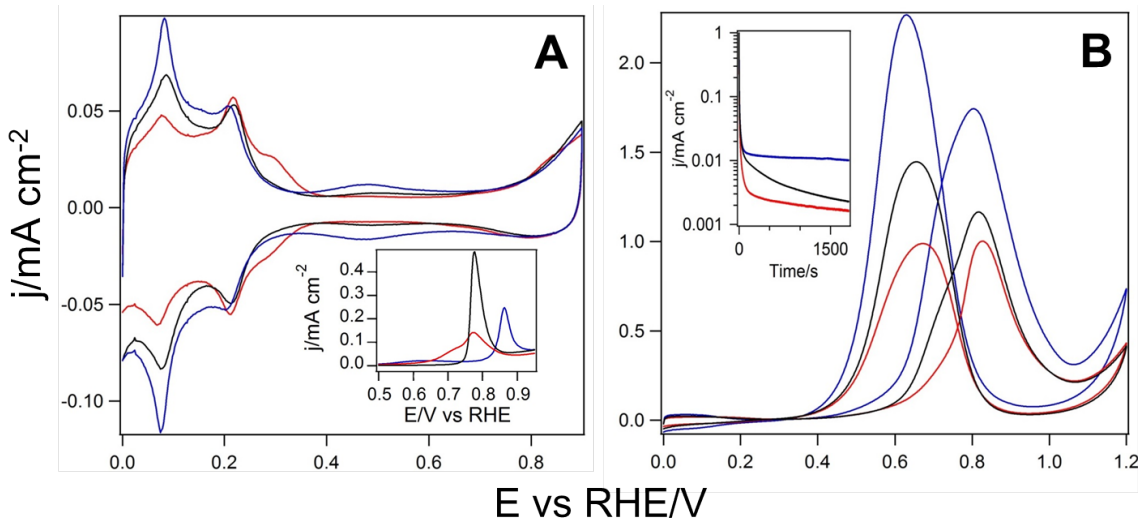

Figure 5. Normal CVs in 0.5 M H_2SO_4 (A) and MOR CVs in 0.5 M H_2SO_4 + 0.5 M CH_3OH (B) of the Pt black (black), cubic (red) and O/T (blue) Pt NPs. The higher peak currents for the negative scans had to do with that the NP surface started with no CO poisoning while this was not the case for the positive scans. Insets show the gaseous CO oxidation in 0.5 M H_2SO_4 (A) and the CA measurements over 1800 s at 0.5 V in 0.5 M H_2SO_4 + 0.5 M CH_3OH (B).

The COR of gaseously adsorbed CO_{ads}, commonly referred to as CO stripping, on the Pt black, cubic and O/T Pt NPs in 0.5 M H_2SO_4 are displayed in the inset of Figure 5A. The peak potentials are 0.78 V, 0.76 V and 0.86 V for the Pt black, cubic and O/T Pt NPs, respectively with the earliest onset of oxidation occurring on the cubic Pt NPs at 0.60 V, which is *ca.* 200 mV earlier than the other two samples. As observed previously, the O/T Pt NPs required the highest potential to oxidize CO_{ads}, while the cubic Pt NPs showed the broadest peak widths.[8] The low onset of the COR on the cubic Pt NPs in contrast to the difficulty of oxidation on the O/T Pt NPs would suggest that the cubic Pt NPs be more active in the MOR than the O/T NPs.

Upon investigation, however, the intrinsic activity trends for the MOR are not corresponding to the COR trend, which is apparent from the MOR CVs displayed in Figure 5B. Notably, both the CV and CA measurements showed that the O/T Pt NPs had the highest MOR activity, followed sequentially by the Pt black and cubic Pt NPs. This is the same order as observed previously on the shape-controlled Pt NPs,[8, 10] but different from the single crystal surfaces.[5, 10, 32]

Notice that the higher backward potential scan peak current is much higher than that of the forward scan for the O/T Pt NPs. This was caused by the relatively low up potential limit in an attempt to alter less the surface structure. Because of lower up potential limit, the oxidized Pt surface could be reduced at a higher potential on the backward scan, which led to a small potential window in which the Pt surface was largely reduced but not yet poisoned severely by the CO thus higher peak current.

Returning briefly to the activity dependence of surface orientation on the presence or absence of PVP, we shall compare data obtained using the Pt black as a reference (by setting its values to 1). The activity enhancements in the order of O/T:black:cubic Pt NPs as measured in Figure 5B are 1.5:1:0.97 in CV (using the peak currents of positive scans) and 4.5:1:0.32 in CA (using the currents measured at 1800s, inset in Figure 5B), respectively. These PVP-free values compared to the corresponding values for the shape-controlled Pt NPs with residual PVP[8] were 2.9:1:0.46 in CV and 12:1:0.15 in CA, respectively. Interestingly, the MOR activity of the PVP-free O/T Pt NPs is about half of the O/T Pt NPs with residual PVP, while that of the PVP-free cubic Pt NPs is about twice of the PVP-protected cubic Pt NPs.. In other words, the presence of PVP enhances the MOR activity on the O/T Pt NPs, but suppresses the activity on the cubic Pt NPs as compared to the PVP-free counterparts. Notice that even without residual PVP, *i.e.* only based on the morphology, the O/T Pt NPs showed ~50% increase in the MOR activity as compared to the commercial Pt black.

3.3. ATR–SEIRAS Characterization

3.3.1. CO Oxidation Reaction. The potential difference spectra for the oxidation of gaseous CO_{ads} in 0.5 M H_2SO_4 on the Pt black, O/T and cubic Pt NPs during potential stair-step measurements with a 0.1V potential step from 0V to 1.2V are displayed in Figure 6 with 1.2V as the reference. The spectra exhibit the characteristic linearly bound CO (CO_L) and bridge bound

CO (CO_B) with frequency ranges from *ca.* 2000 cm^{-1} to 2050 cm^{-1} and *ca.* 1850 cm^{-1} to 1900 cm^{-1}, respectively, independent of surface structure. Note the amount of bridge bound CO, however, was much higher here on the PVP-free NPs than that on the PVP-protected shape-controlled Pt NPs, which is most likely a manifestation of the availability of vicinal Pt sites on the clean PVP-free surface.[33] The small band centered about 1700 cm^{-1} on the O/T and cubic Pt NPs can be assigned to multi-bound CO (CO_M).[34] There is a strong bending water vibrational band on the Pt surfaces between 1610 cm^{-1} and 1615 cm^{-1} labeled as δ(HOH) that is strongest on the Pt black and weakest on the cubic Pt NPs.

Additional confirmation of surface cleanliness is seen by the comparable spectral features on the Pt NPs to Pt black, *i.e.* the absence of polymeric bands. PVP has been shown to interact mostly through the carbonyl, >C=O, group on the surface of Pt.[35] If the polymer were present, the >C=O stretch vibration would exhibit a prominent IR band between 1660 cm^{-1} and 1680 cm^{-1} as previously reported.[22] No such band was observed on the PVP-free Pt surfaces studied here.

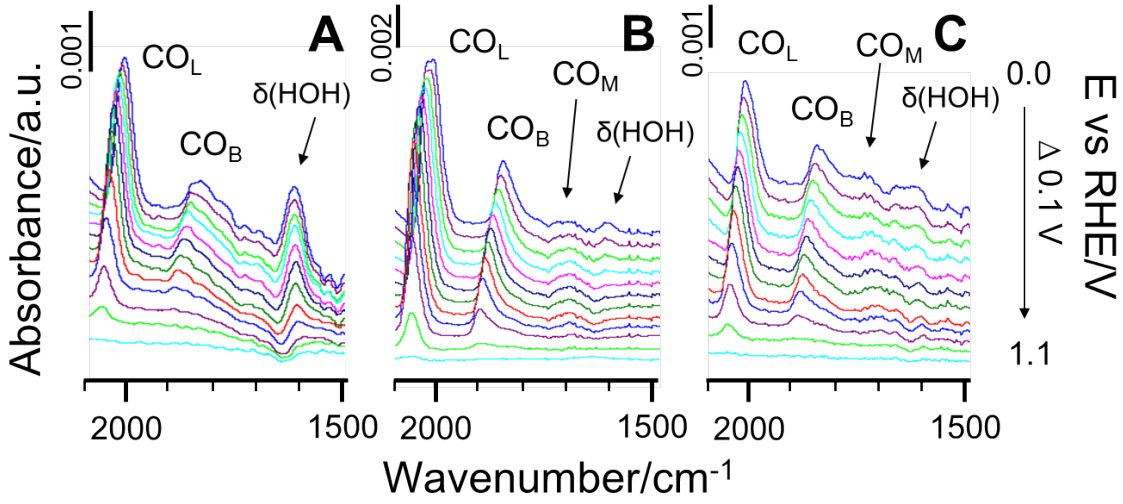

Figure 6. Potential dependent ATR–SEIRAS spectra for gaseously adsorbed CO on the Pt black (A), O/T (B) and cubic (C) Pt NPs in 0.5 M H_2SO_4 with the reference spectra recorded at 1.2 V.

Figure 7 summaries the COR trends for the normalized (by the respective ECSA) integrated band intensities for the CO_L, CO_B and δ(HOH) on the Pt NPs as a function of the

applied potential in 0.5M H_2SO_4 (A-C). In contrast to the PVP-protected shape-controlled samples studied previously, where the gaseously adsorbed CO behaved quite differently for different samples,[33] the gaseous CO adsorbed on the PVP-free samples and Pt black showed very similar behavior (see Figure 7) even though the three had distinctly different surface structures (see Figure 4). All three samples showed the same vibrational frequency range of CO_{ads} as a function of the electrode potential and the O/T sample had basically the same Stark tuning rates as those of the Pt black while those of the cubic sample were somewhat smaller (Figure 7D). The CO_L was more easily oxidized than CO_B as noted in previous studies with Pt.[36, 37] The decrease in the amplitude of δ(HOH) in the stair-step experiments corresponds well with the oxidation of CO_{ads} that is expected to consume interfacial water as has been reported.[22] The CO_L band intensity also decreased slightly below *ca.* 0.6V in the so-called pre-ignition region before the rapid decrease signals quick oxidation or the ignition region. Simultaneously, the CO_B intensity remained largely unchanged until the swift oxidation occurred beyond *ca.* 0.6V. Interestingly, the band intensity of the CO_B on the cubic Pt NPs increased at *ca.* 0.4V that was corresponding to the pre-ignition occurring with CO_L, which suggests a possible CO conversion process. Moreover, the lack of a δ(HOH) band near 1630 cm^{-1} indicates that the interfacial water was substantially hydrogen bonded.[38]

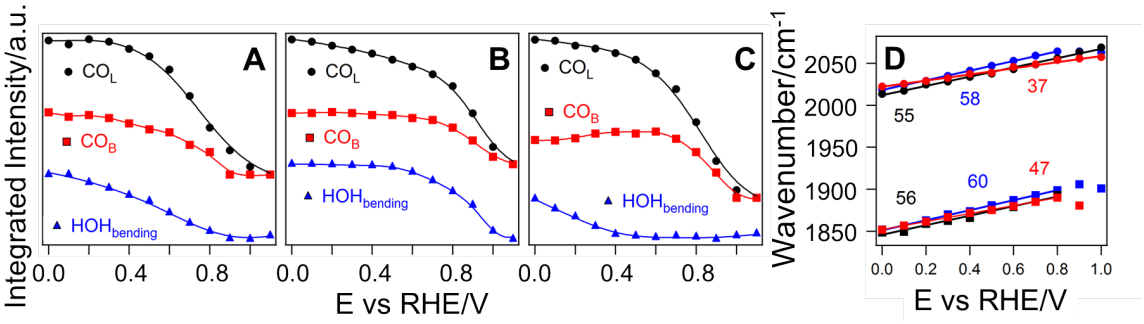

Figure 7. Normalized (by ECSA) integrated band intensities as a function of applied potential for linear (CO_L), bridged (CO_B) and bending water ($HOH_{bending}$) during the COR on the Pt black (A), O/T (B) and cubic (C) Pt NPs in 0.5 M H_2SO_4. Corresponding potential dependent

frequencies of the CO_L (circle) and CO_B (square) on the Pt black (black), O/T (blue) and cubic (red) Pt NPs in 0.5 M H_2SO_4 (D).

As mentioned above, the potential dependent frequency shifts showed much more similar behavior for CO_L and CO_B on the PVP-free surfaces, as shown in Figure 7D, than that on the surfaces having residual PVP.[33] One noticeable difference is that the CO adsorbed on the cubic Pt NPs showed lower tuning rates of 37 and 47 cm^{-1} V^{-1} for CO_L and CO_B, respectively, in 0.5M H_2SO_4 than the 55 and 58 cm^{-1} V^{-1} for the Pt black and O/T Pt NPs, respectively. Overall, despite the evidence for clearly different surface arrangements and in turn the catalytic activities, there was little variability detected by ATR–SEIRAS for the gaseously adsorbed species at the high coverage of CO_{ads} during the CO stripping measurements. This observation was somewhat anticipated since the NPs were composed of Pt metal with low index planes without electronic and/or geometric effects induced by the surfactant.

3.3.2. Methanol Oxidation Reaction. The potential dependent spectra displayed in Figure 8 summarize the MOR on the Pt black, O/T and cubic Pt NPs during the stair-step measurements from 0V to 1.2V to 0V with a 0.1V potential step. Spectra between 1500 cm^{-1} to 2100 cm^{-1} shown in Figure 8A–C are referenced to the upper potential of 1.2V, which is shown as a flat line in the middle of the stacked spectra. In contrast to the gaseous CO stripping spectra, the CH_3OH-generated CO_{ads} exhibits a lone CO_L band between 2000 cm^{-1} and 2060 cm^{-1}, except on the cubic Pt NPs that display an additional minor peak at *ca.* 1700 cm^{-1}. This strongly implies that the

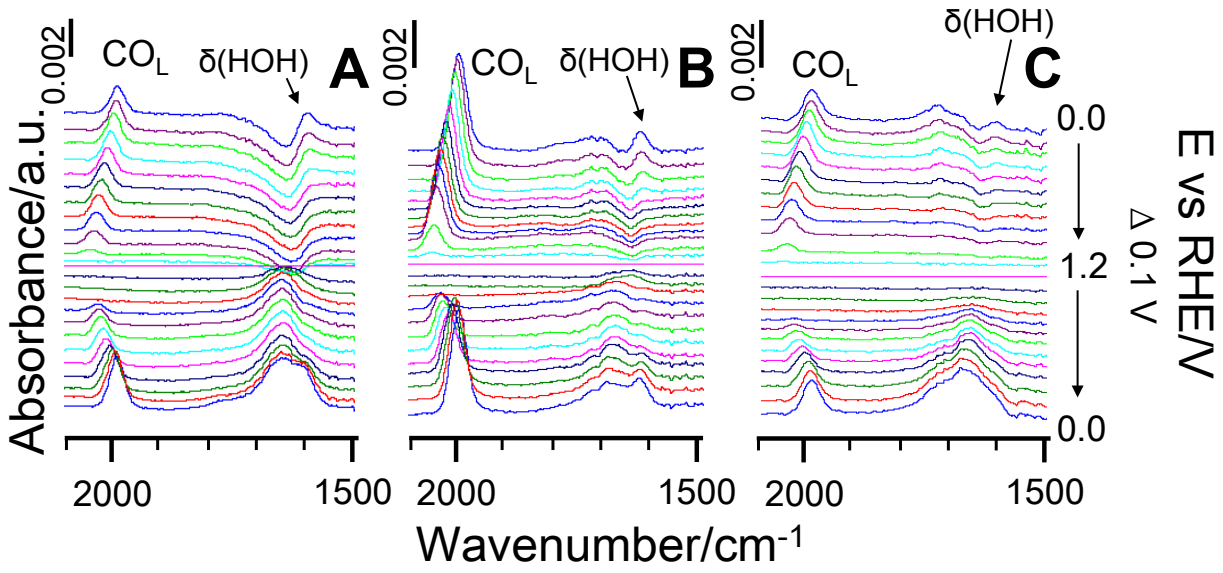

Figure 8. Potential dependent ATR–SEIRAS spectra recorded during the MOR on the Pt black (A), O/T (B) and cubic (C) Pt NPs in 0.5 M H_2SO_4 + 0.5 M CH_3OH with the reference spectra recorded at 1.2V.

methanol carbon probably bound to the surface only as an atop configuration during the dehydrogenations. Adsorbed methanol, CH_3OH_{ads}, was also detectable at *ca.* 1015 cm^{-1} on the Pt NPs similar to that observed on the commercial samples previously.[28] Moreover, there are two δ(HOH) bands observed during the MOR at *ca.* 1610 cm^{-1} and *ca.* 1650 cm^{-1}. The former is assigned to the surface adsorbed interfacial water as in the previous section, while the latter has been attributed to the bending of the bulk water.[39, 40] In the following, we will focus only on the interfacial water.

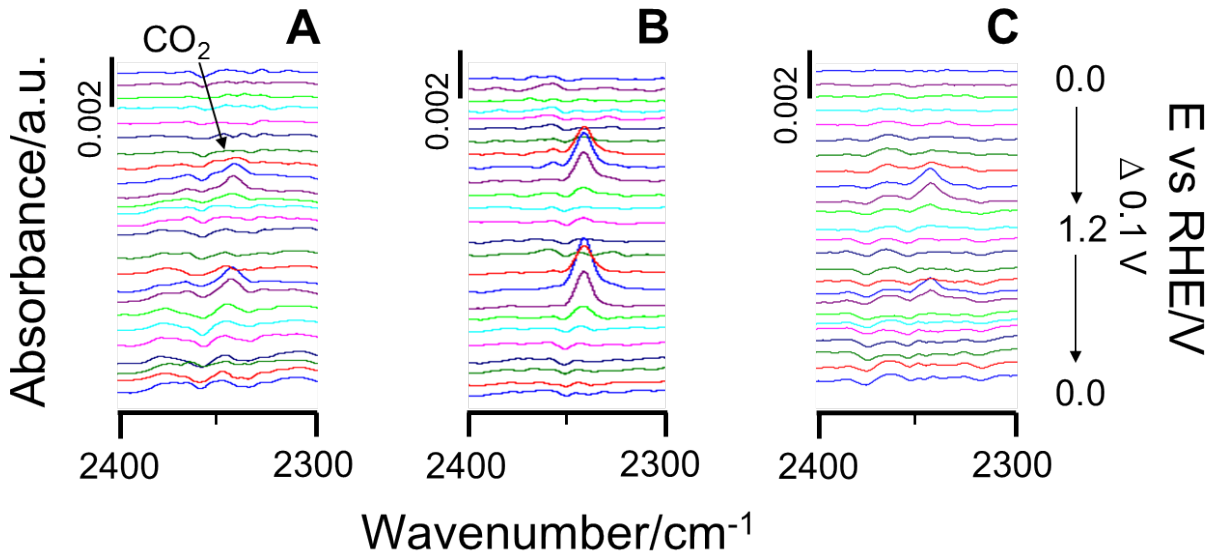

Figure 9. Potential dependent ATR–SEIRAS spectra of CO_2 produced during the MOR on the Pt black (A), O/T (B) and cubic (C) Pt NPs in 0.5 M H_2SO_4 + 0.5 M CH_3OH with the reference spectra recorded at 0.0 V.

Moreover, as shown in Figure 9, the production of CO_2 can be observed albeit the molecule can diffuse away from the surface in the ATR-SEIRAS setting. Nonetheless, a direct correlation of the oxidized CO_{ads} and CO_2 was possible as shown in Figure 10, which is consistent with previous works using the thin-layer approach.[21] Again, the MOR-generated CO_{ads} showed very similar behavior on the PVP-free samples in terms of the vibration frequency at a given electrode potential, overall frequency range, and Stark tuning rates that are surprisingly so close to those for the gaseous CO_{ads} (Figure 7D). Again, this is in contrast to PVP-protected,[33] where different vibrational frequencies at a given electrode potential were observed for the three samples and different corresponding Stark tuning rates were noted..[33] Since the Stark tuning rates for the anodic (Ano) and cathodic (Cath) directions are almost the same, this indicates that the CO_{ads} was generated in the same way independent of the direction of electrode potential scan during the MOR. Moreover, since they are also very close to those of gaseously adsorbed CO (Figure 7D) also implies that the MOR-generated CO_{ads} formed closely packed islands. This suggests that the linearity of the Stark tuning was maintained beyond the peak potentials of CO_2

production meaning that the COR took place mainly at the peripheries of the CO_{ads} islands as it implies that the local coverage of the remaining CO_{ads} was maintained.

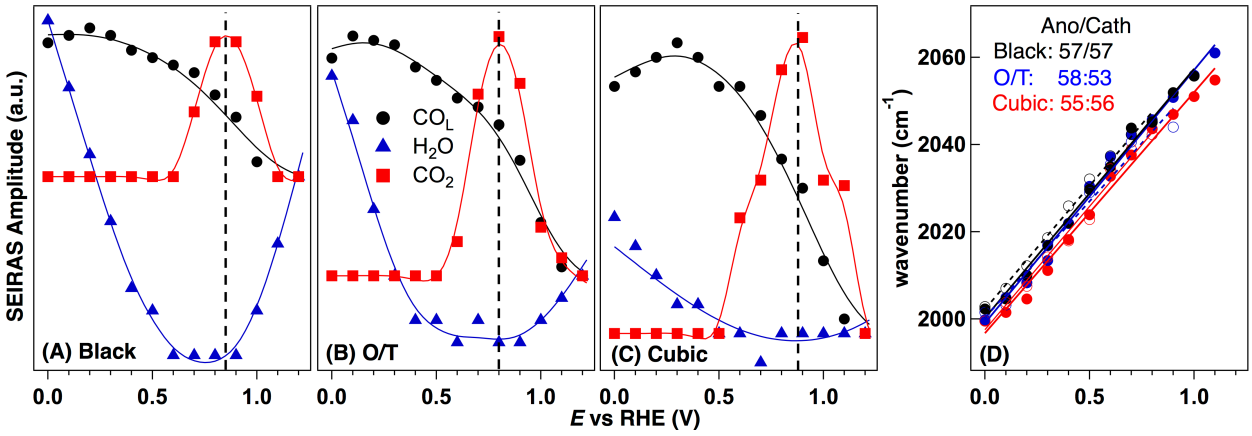

Figure 10. Normalized peak intensities as a function of applied potential for linear CO (black circles), interfacial bending water (blue triangles) and CO_2 (red squares) during the MOR on the Pt black (A), O/T (B) and cubic (C) Pt NPs in 0.5 M H_2SO_4. Corresponding potential dependent frequencies of the anodic CO_L (solid–circle) and cathodic CO_L (open–circle) on the Pt black (black), O/T (blue) and cubic (red) Pt NPs (red) in 0.5 M H_2SO_4 (D).

Alternatively, the peak potential for the CO_2 production for the O/T Pt NPs was about 50mV and 90mV less positive than those for the Pt black and cubic Pt NPs respectively (red squares and the vertical dashed lines in Figure 10A to 10C), which is in agreement with the EC observation of the enhanced MOR on the former (Figure 5B). The *in situ* SEIRAS data, however, do not provide a clearly distinguishable evidence as to what is the exact mechanism for the MOR enhancement observed on the PVP-free O/T Pt NPs. One plausible indication may be gleaned by the rate of decrease of the interfacial water during the MOR by following the band at 1610 cm^{-1} as presented in Figure 10A to 10C (blue triangles). The O/T Pt NPs showed the fastest decrease as the electrode potential scanned positively, followed in the respective order by Pt black and cubic Pt NPs, suggesting that the interfacial water may play a differentiating role here.

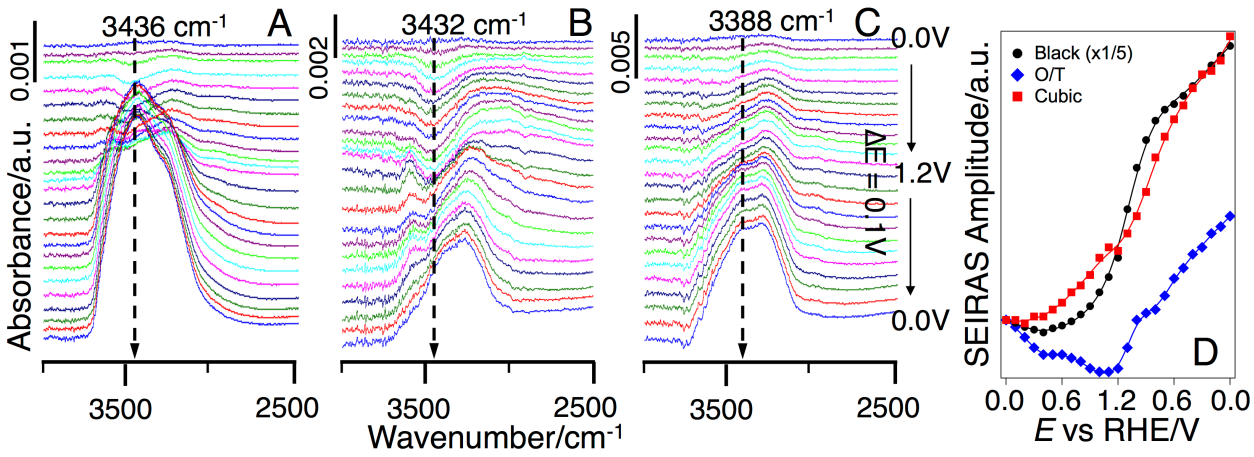

Figure 11. Potential dependent ATR–SEIRAS spectra of the water stretching vibrations (υ(OH)) during the MOR on Pt black (A), Pt (111) NCs (B) and Pt (100) NCs (C) in 0.5 M H_2SO_4 + 0.5 M CH_3OH with the reference spectra recorded at 0.0 V. (D) The SEIRAIS amplitude as a function of electrode potential at the respective frequencies indicated by the dashed arrows for Pt black (circles), O/T (diamonds), and cubic (cubes) Pt NPs.

It was observed previously[41] that among the three possible types of interracial water, *i.e.* the strongly hydrogen-bound (~3200 cm^{-1}), weakly hydrogen-bound (~3400 cm^{-1}), and non-hydrogen-bound water (~3600 cm^{-1}), the weakly hydrogen-bound water was identified as the active water species that participates the MOR as the oxygen-containing species. Figure 11 presents the water stretching vibrational bands for the Pt black (A), O/T (B), and cubic Pt NPs observed during the MOR stair-step measurements as those in Figures 8 and 9. For the O/T and Pt black samples, there was indeed a well-defined, negative going peak at ~3435 cm^{-1} (indicated by the corresponding dashed arrows in Figure 11A and 11B) during the first positive potential scan. By the end of the negative potential scan, this peak eventually became a positive-going peak for the Pt black, but a less well-defined shoulder for the O/T Pt NPs. For lack of a such well-defined peak for the cubic sample during the positive potential scan, the spectral shoulder at 3388 cm^{-1} in the IR spectrum recorded at the end of the negative potential scan, as indicated by the dashed arrow in Figure 11C, was used to define and gauge the behavior of the weakly hydrogen-bound water in this sample.

When the respective SEIRAS amplitudes at these frequencies as a measure of the weakly hydrogen-bounded water are plotted as a function of the electrode potential during the stair-step measurements, as presented in Figure 11D, it becomes clear that the O/T sample behaved distinguishably different from the Pt black and cubic samples. The much larger variation in the IR amplitude of the weakly hydrogen-bound water observed on the former sample during the positive potential scan can be taken as an evidence of having more such type of interfacial water available on the sample surface for the MOR thus leading to higher activity. Although, the continuous increase in IR amplitude during the subsequent negative potential scan is not well understood at this moment. Using the variation in IR amplitude during the positive potential scan as a measure for the MOR activity, one would expect that the cubic sample have the least activity and the Pt black sit in the middle, which is exactly what was observed electrochemically (Figure 5B).

4. Conclusions

In summary, the purpose of this investigation was to distinguish the PVP effect from the nanoscale surface orientation effect of the shape-controlled Pt NPs on the MOR activity. This was made possible by our optimizing a UV-based treatment of the as-synthesized Pt NPs that can completely eliminate the strongly surface-bound PVP and produce PVP-free shape-controlled Pt NPs. It was observed that the O/T Pt NPs could enhance MOR by ~50% as compared to the commercial Pt black while the cubic Pt NPs had slightly lower MOR activity than the latter. By comparing to the MOR activity data available on the similar shape-controlled Pt NPs, but in the presence of PVP, it was concluded that the surface-bound residual PVP further enhances the MOR activity on the O/T Pt NPs, but suppresses it on the cubic particles. The *in situ* SEIRAS study of the MOR on the PVP-free shape-controlled Pt NPs strongly suggests that the observed

enhancement in MOR was probably related to more weakly hydrogen-bound water available on the surface of the O/T sample than on the other two samples. While this is in agreement with previous observation[41] that has identified the weakly hydrogen-bound interfacial water as the active oxygen-containing species for the MOR, it is mechanistically different from the PVP effect that has more to do with enabling a different (*i.e*. direct) reaction pathway.[21, 33] Further mechanistic investigation into the reason for PVP displays selective MORenhancement on the O/T, but suppresses activity on the cubic Pt NPs is warranted and being pursued in our laboratory.

Acknowledgements

This research has been supported by the NSF (CHE-0923910) and the DOE (DE-FG02-07ER15895). A.M.L. received support from the NSF (OISE–1130454) and C.L.R. was supported by a GUROP 2013 summer research grant. TEM images were taken at the NISP Lab at UMD at College Park, MD.

References:

1. J. L. Cohen, D. J. Volpe and H. D. Abruna, *Phys. Chem. Chem. Phys.*, 2007, **9**, 49-77.
2. T. H. M. Housmans, A. H. Wonders and M. T. M. Koper, *J. Phys. Chem. B*, 2006, **110**, 10021-10031.
3. M. Neurock, M. Janik and A. Wieckowski, *Faraday Discussions*, 2009, **140**, 363-378.
4. E. Herrero, K. Franaszczuk and A. Wieckowski, *J. Phys. Chem.*, 1994, **98**, 5074-5083.
5. N. M. Markovic and P. N. Ross Jr, *Surf. Sci. Rep.*, 2002, **45**, 117-229.
6. J. Solla-Gullon, F. J. Vidal-Iglesias and J. M. Feliu, *Annual Reports Section "C" (Physical Chemistry)*, 2011, **107**, 263-297.
7. Y.-W. Lee, S.-B. Han, D.-Y. Kim and K.-W. Park, *Chem. Commun.*, 2011, **47**, 6296-6298.
8. C. Susut, G. B. Chapman, G. Samjeske, M. Osawa and Y. Y. J. Tong, *Phys. Chem. Chem. Phys.*, 2008, **10**, 3712-3721.
9. N. Tian, Z.-Y. Zhou, S.-G. Sun, Y. Ding and Z. L. Wang, *Science*, 2007, **316**, 732-735.
10. J. Solla-Gullon, F. J. Vidal-Iglesias, A. Lopez-Cudero, E. Garnier, J. M. Feliu and A. Aldaz, *Phys. Chem. Chem. Phys.*, 2008, **10**, 3689-3698.
11. T. S. Ahmadi, Z. L. Wang, T. C. Green, A. Henglein and M. A. El-Sayed, *Science*, 1996, **272**, 1924-1925.
12. F. J. Vidal-Iglesias, R. M. Arán-Ais, J. Solla-Gullón, E. Herrero and J. M. Feliu, *ACS Catal.*, 2012, **2**, 901-910.

13. Z.-Y. Zhou, N. Tian, J.-T. Li, I. Broadwell and S.-G. Sun, *Chem. Soc.Rev.*, 2011, **40**, 4167-4185.
14. G. Fu, K. Wu, X. Jiang, L. Tao, Y. Chen, J. Lin, Y. Zhou, S. Wei, y. tang, T. Lu and X. Xia, *Phys. Chem. Chem. Phys.*, 2013.
15. A. X. Yin, X. Q. Min, Y. W. Zhang and C. H. Yan, *J. Am. Chem. Soc.*, 2011, **133**, 3816-3819.
16. Z. Peng, C. Kisielowski and A. T. Bell, *Chem. Commun.*, 2012, **48**, 1854-1856.
17. B. N. Johnson and R. Mutharasan, *J. Phys. Chem. C*, 2013, **117**, 1335-1341.
18. J. Monzo, M. T. M. Koper and P. Rodriguez, *ChemPhysChem*, 2012, **13**, 709-715.
19. M. Crespo-Quesada, J.-M. Andanson, A. Yarulin, B. Lim, Y. Xia and L. Kiwi-Minsker, *Langmuir*, 2011, **27**, 7909-7916.
20. P. Rodriguez, E. Herrero, J. Solla-Gullon, F. J. Vidal-Iglesias, A. Aldaz and J. M. Feliu, *Electrochim. Acta*, 2005, **50**, 4308-4317.
21. C. Susut, D.-J. Chen, S.-G. Sun and Y. J. Tong, *Phys. Chem. Chem. Phys.*, 2011, **13**, 7467-7474.
22. A. M. Hofstead-Duffy, D.-J. Chen and Y. J. Tong, *Electrochim. Acta*, 2012, **82**, 543-549.
23. H. Song, F. Kim, S. Connor, G. A. Somorjai and P. Yang, *J. Phys. Chem. B.*, 2004, **109**, 188-193.
24. C. Susut, T. D. Nguyen, G. B. Chapman and Y. Tong, *Electrochim. Acta*, 2008, **53**, 6135-6142.
25. B. E. Conway and G. Jerkiewicz, *J. Electroanal. Chem.*, 1992, **339**, 123-146.
26. M. Osawa, *Bull. Chem. Soc. Jpn.*, 1997, **70**, 2861-2880.
27. D. J. Chen, A. M. Hofstead-Duffy, I. S. Park, D. O. Atienza, C. Susut, S. G. Sun and Y. Y. J. Tong, *J. Phys. Chem. C.*, 2011.
28. A. M. Hofstead-Duffy, D.-J. Chen, S.-G. Sun and Y. Y. J. Tong, *J. Mater. Chem.*, 2012, **22**, 5205-5208.
29. H. Miyake, S. Ye and M. Osawa, *Electrochem. Comm.*, 2002, **4**, 973-977.
30. F. J. Vidal-Iglesias, J. Solla-Gullon, E. Herrero, V. Montiel, A. Aldaz and J. M. Feliu, *Electrochem. Commun.*, 2011, **13**, 502-505.
31. D. S. Gatewood, T. L. Schull, O. Baturina, J. J. Pietron, Y. Garsany, K. E. Swider-Lyons and D. E. Ramaker, *J. Phys. Chem. C*, 2008, **112**, 4961-4970.
32. X. H. Xia, T. Iwasita, F. Ge and W. Vielstich, *Electrochim. Acta*, 1996, **41**, 711-718.
33. A. M. Levendorf, S.-G. Sun and Y. Y. J. Yong, *Electrocatal.*, 2014, DOI: 10.1007/s12678-014-0186-1.
34. H. Miyake, T. Okada, G. Samjeske and M. Osawa, *Phys. Chem. Chem. Phys.*, 2008, **10**, 3662-3669.
35. Y. Borodko, S. E. Habas, M. Koebel, P. Yang, H. Frei and G. A. Somorjai, *J. Phys. Chem. B.*, 2006, **110**, 23052-23059.
36. G. SamjeskeÌ , K.-i. Komatsu and M. Osawa, *J. Phys. Chem. C*, 2009, **113**, 10222-10228.
37. Y.-G. Yan, Y.-Y. Yang, B. Peng, S. Malkhandi, A. Bund, U. Stimming and W.-B. Cai, *J. Phys. Chem. C*, 2011, **115**, 16378-16388.
38. M. Osawa, M. Tsushima, H. Mogami, G. Samjeske and A. Yamakata, *J. Phys. Chem. C*, 2008, **112**, 4248-4256.
39. K.-I. Ataka and M. Osawa, *Langmuir*, 1998, **14**, 951-959.
40. Yan, Q.-X. Li, S.-J. Huo, M. Ma, W.-B. Cai and M. Osawa, *J. Phys. Chem. B*, 2005, **109**, 7900-7906.

41. D. J. Chen, A. M. Hofstead-Duffy, I. S. Park, D. O. Atienza, C. Susut, S. G. Sun and Y. Y. J. Tong, *J. Phys. Chem. C.*, 2011, **115**, 8735-8743.

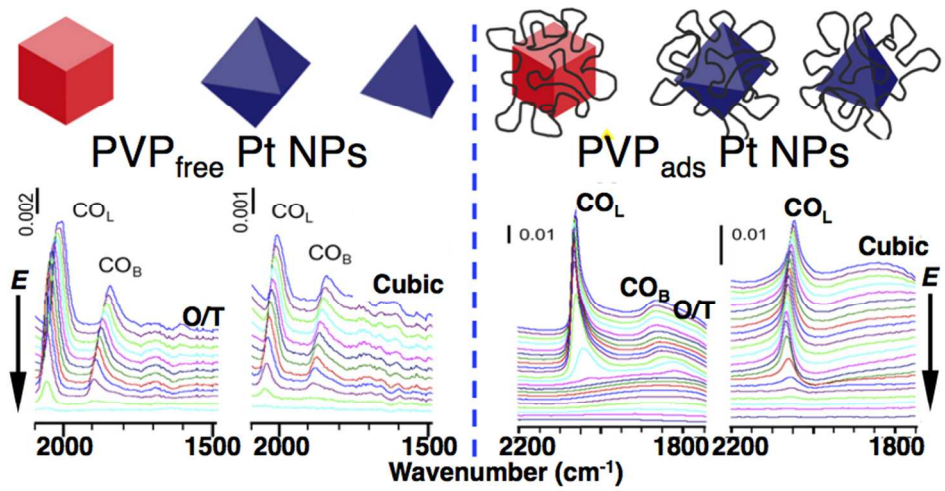

The adsorbed PVP enhances further the MOR activity on the O/T but suppresses it on the cubic Pt NPs.